Cite this: DOI: 10.1039/c0xx00000x

www.rsc.org/xxxxxx

ARTICLE TYPE

Vertically-Aligned ZnO Nanorods Doped with Lithium for Polymer Solar Cells: Defect Related Photovoltaic Properties

Pipat Ruankham, Takashi Sagawa,* Hiroshi Sakaguchi and Susumu Yoshikawa*

Received (in XXX, XXX) Xth XXXXXXXXX 20XX, Accepted Xth XXXXXXXXX 20XX

DOI: 10.1039/b000000x

The nanorod arrays of ZnO incorporated with lithium atoms show specific crystallinity, photoluminescence and absorption properties, which are promising for the improvement of photovoltaic performance of hybrid solar cells based on ZnO/poly(3-hexylthiophene). Li ions can be incorporated into ZnO crystals during the hydrothermal growth of the nanorods. The presence of Li in ZnO crystal was confirmed through X-ray diffraction analysis and by the photoluminescence spectra obtained. The difference in photovoltaic properties brought about by Li doping were determined from concentrations of the precursor solution. It was determined that appropriate Li doping improves both the short circuit current density (J_{sc}) and open circuit voltage (V_{oc}). The quenching of photoluminescence of Li-doped ZnO nanorods/P3HT films indicates effective charge transfer at the interface due to oxygen-enrichment surface, corresponding to the enhancement of J_{sc}. The improvement of V_{oc} was due to the suppression of the charge injection from the electrode brought about by the increase in barrier height at the ITO/ZnO interface as the work function of the ZnO nanorods was reduced after Li ion doping. However, further substitution of Li to Zn (Li_{Zn}) lead to increased reverse current densities of minority carriers decreasing V_{oc} after the maximum value at 5 atom% incorporation. The maximum power conversion efficiency of 0.37% was obtained at 5 atom% doping, although improvements in photovoltaic performances through Li doping was still be seen up to 20 atom% doping.

Introduction

Hybrid polymer-metal oxide solar cells have been widely investigated in recent years due to their low-cost manufacturing. However, the power conversion efficiencies of hybrid devices are commonly low. Efforts to improve device performance have focused on the fabrication of inorganic nanostructured materials,[1] the modification of the interface[2] between the polymer and the metal electrode and band-offset engineering.[3] One of the most widely studied inorganic semiconductors for electronic devices is zinc oxide because of its wide band gap, good carrier mobility and great variety of morphologies.[4] The vertically-aligned ZnO nanorods structure has great potential for hybrid solar cells and other photo electronic devices. Of the various methods to prepare ZnO nanostructures, hydrothermal growth has been favored since it is simple, inexpensive, and prepared at low temperatures. One of the challenges in hydrothermal preparation is to dope foreign atoms into well-aligned ZnO nanorods during growth to improve their electric properties. Here, we introduce lithium atoms and confirm their presence in the crystal of ZnO nanorods. Because the acceptor level of Li has a small binding energy (Li_{Zn})[5] and Li is highly soluble in ZnO[6], the incorporation of Li atoms into ZnO nanorods can be possible. However, lithium can easily occupy interstitial position (Li_i) due to its small ionic radius. This Li_i acts as donor[5] and can compensate the acceptor action.[7]

Most of the hybrid inorganic-organic devices have low photovoltaic performance due to the large band offset between the electron donor and acceptor materials [3] and inefficient charge generation and charge transport at their interface. In our previous work, we introduced the modification of the surface of the metal oxide by N719 dye, which resulted to the enhancement of electron injection from polymer to metal oxide.[2] In this context, we have now succeeded in doping Li atoms into ZnO crystal during hydrothermal growth. Li incorporation is promising to improve the power conversion efficiency of hybrid polymer/metal oxide solar cells constructed from vertically-aligned ZnO nanorod arrays as the electron transporting layer and poly(3-hexylthiophene) (P3HT) as the donor. We establish properties of Li-doped ZnO nanorod arrays prepared through a hydrothermal method and examine the influence of Li impurities on photovoltaic performance of hybrid solar cells.

Experimental

Materials

Zinc acetate ($Zn(CH_3COO)_2$), zinc nitrate hexahydrate ($Zn(NO_3)_2 6H_2O$), lithium acetate ($Li(CH_3COO)$), lithium nitrate ($LiNO_3$), monoethanolamine ($H_2NCH_2CH_2OH$), and chlorobenzene (C_6H_5Cl) were purchased from Wako Pure Chemical Industries, Japan. Hexamethylenetetramine ($C_6H_{12}N_4$) and 2-methoxyethanol ($C_2H_8O_2$) were bought from Aldrich.

P3HT was purchased from Rieke Metals. Indium tin oxide (ITO)-coated glass (10 Ω cm^{-2}) was purchased from Geomatec, Japan. The substrates were cleaned prior to use by ultrasonic agitation in distilled water, acetone and isopropanol.

Synthesis of Li-doped ZnO Nanorods

$Zn_{1-x}Li_xO$ (x = 0 - 0.25) nanopowder thin films that served as seed layers were deposited on ITO substrates by spin coating $Zn_{1-x}Li_x$ acetate solution (0.3 M). This solution was prepared by controlling the molar ratio of zinc acetate to lithium acetate with monoethanolamine (0.3 M) as the complexing agent and 2-methoxyethanol as the solvent. Note that the value of x in this literature refers to the concentration of the dopant precursor. Then, the films were annealed at 300 °C for 10 min. This process was repeated twice, yielding films with thicknesses of approximately 30 nm. The hydrothermal growth of Li-doped ZnO nanorod arrays was performed by suspending the as-prepared ZnLiO substrates in a polypropylene container filled with aqueous solution of zinc nitrate hexahydrate, lithium nitrate and hexamethylenetetramine (50 mM). The container was then aged in an oil bath at 90 °C for 25 min. The substrate was carefully rinsed by distilled water for several times and finally annealed at 150 °C for 10 min to remove organic residues from inorganic materials.

Fabrication of Hybrid Solar Cells

A solution of P3HT in chlorobenzene (30 mg ml^{-1}) was spin-coated on top of ZnO nanorods, yielding a thickness of P3HT (including the length of the nanorod) about 230 nm. Subsequently, the films were annealed at 150 °C in an Ar-filled glove box for 3 min. Finally, the Ag top electrode (100 nm) was thermally evaporated using a vacuum evaporation system.

Characterization

An electron energy-loss spectrum in a scanning transmission electron microscope (STEM-EELS) was recorded to investigate the distribution and confirm the presence of Li element in ZnO nanorods. X-ray diffraction spectrometer was preformed to analyze crystalinity of Li-doped ZnO nanorods. Photoluminescence studies were carried out using a He-Cd laser operating at the wavelength of 325 nm. Photo-electron yield spectrometer (PYS) in air was carried out on a Riken Keiki model AC-2. The photocurrent-voltage characteristics were measured under ambient atmosphere and simulated solar light, AM 1.5, 100 mW cm^{-2} on CEP-2000 (Bunkoh-Keiki). A photo mask with the area of 0.0503 cm^2 was used to define active area of the device irradiated by the light. Transmissions and adsorptions spectra were obtained from a UV-vis spectrophotometer (UV-2450 Shimadzu).

Results and Discussions

Properties of Li-doped ZnO nanorods

The $Zn_{1-x}Li_xO$ (x = 0 - 0.25) nanorods thin films were prepared by sol-gel-hydrothermal growth form a solution of $Zn_{1-x}Li_x$ acetate and $Zn_{1-x}Li_x$ nitrate with a proper molar ratio. The $Zn_{1-x}Li_xO$ nanorod arrays deposited on ITO substrates were investigated with electron energy-loss spectroscopy in a scanning transmission electron microscope, STEM-EELS, (Fig. S1, ESI†)

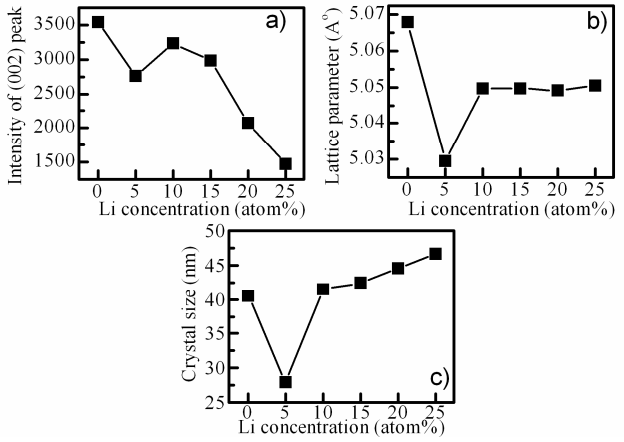

Fig. 1 The variation of a) (002) peak intensity, b) lattice parameter *c*, and c) crystal size of ZnO nanorods doped by various Li concentration.

in order to determine the distribution of Li element in ZnO nanorods. The Li element mapping images confirm the incorporation of Li into ZnO crystals during hydrothermal growth, and indicate a Li-rich phase on the top of ZnO nanorods. It can be suggested that the formation of ZnO crystals dominates over Li incorporation at the beginning of the growth. But when the concentration of Zn ions in solution decreases, the reaction rate slow down, allowing for the Li ions to diffuse into the ZnO crystals.

The XRD patterns (Fig. S2, ESI†) of ZnO nanorods with different Li-doping concentration on ITO substrates were collected. The (100), (002) and (101) peaks of ZnO indicates that the sample is polycrystalline. The (002) peak shows a strong intensity along with very weak (100) and (101) peaks, corresponding to the wurtzite phase of ZnO. Either metallic zinc or lithium characteristic peaks are not observed from the XRD spectra.

The variations of intensity of (002) peak, lattice parameter and crystal size were analyzed (ESI†) and are shown in Fig. 1. The intensity of (002) peak (Fig. 1a) decreases with increasing Li content, indicating that the crystallinity of the samples is degraded with the presence of Li impurity in the ZnO crystal. At 5 atom % Li-doping concentration, a significant decrease in lattice parameter could be expected when the large Zn^{2+} ions (radius of 0.074 nm) are replaced by the smaller Li^+ ions (radius of 0.060 nm).[8, 9] For higher Li-doping concentration, the lattice parameter increases but is still smaller than that of pure ZnO nanorods. This may be due to either interstitial incorporation of Li^+ ions (Li_i, donor) into the lattice[8] or the formation of electrically inactive Li_{Zn}-Li_i pairs explained by Wardle et al.[5]

The optical properties of $Zn_{1-x}Li_xO$ nanorods were investigated by photoluminescence (PL) spectroscopy. Room temperature PL spectra of all the samples (Fig. S3, ESI†) show two bands in the ultraviolet emission at ~410 nm, which are related to near band-edge excitonic emissions[10] and broadband emission in the range of 500 to 800 nm, which is related to the defects in the ZnO crystal. To investigate the defect-related emission and compare the relative changes of the defects after Li doping, the PL spectra were normalized by the PL intensity near band-edge emissions (410 nm). Then, the normalized PL spectra for 0, 5, and 10 atom% doping were divided into five regions using a Gaussian function. The emissions can be seen in the ultraviolet (P1: ~350-

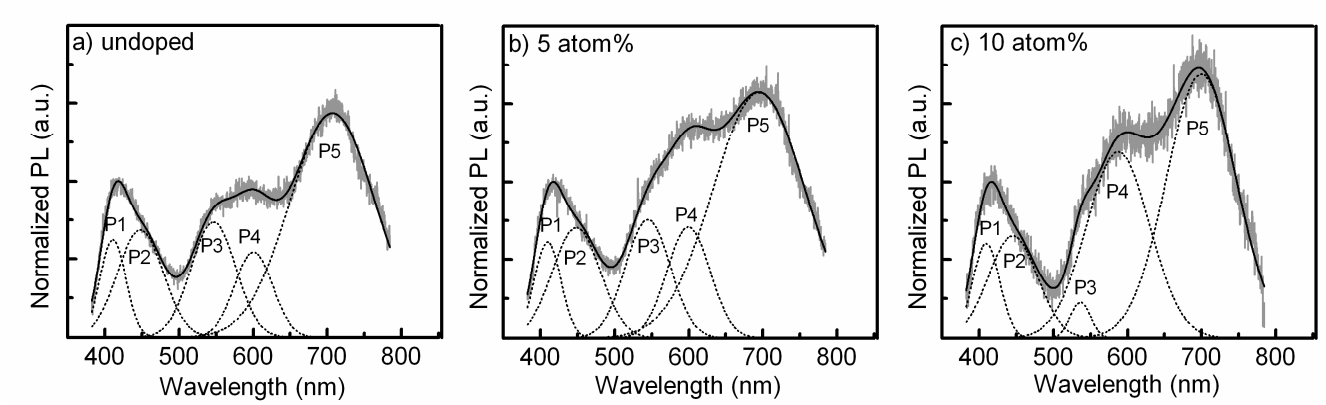

Fig. 2 The normalized of room temperature photoluminescence for $Zn_{1-x}Li_xO$ nanorod films on glass substrates for a) undoped, b) x = 0.05, and c) x = 0.10. The gray solid lines present the experimental data. The P1-P5 (dot lines) denotes the ultraviolet emission, blue emission, green emission, yellow emission, and red emission, respectively. The black solid line is the summation of P1-P5.

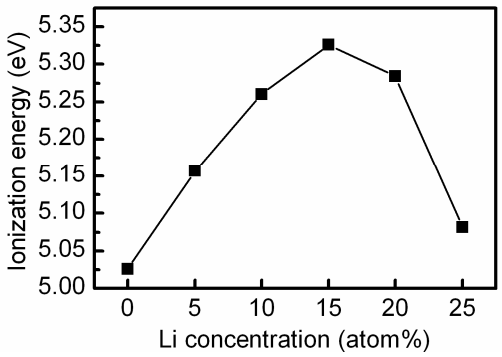

Fig. 3 The first ionization energy (IE) of $Zn_{1-x}Li_xO$ nanorod films.

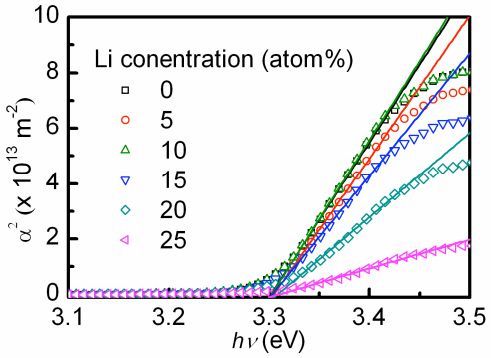

Fig. 4 The plot of absorption coefficient (α) versus photon energy ($h\nu$) for $Zn_{1-x}Li_xO$ nanorod films (x = 0-0.25) on glass substrates. The open symbol and solid line denote the experimental data and fitted curve from equation (ESI†)

450 nm), blue (P2: ~380-500 nm), green (P3: ~480-600 nm), yellow (P4: ~550-650 nm) and red (P5: 580-800 nm) regions, as shown in Fig. 2. The blue emission and green emission have been reported to arise from Zn ions at interstitial sites (Zn_i) of ZnO crystals,[10,11] and oxygen vacancy (V_O),[12, 13, 14] respectively. These emissions were confirmed in the spectra of the pure ZnO sample (Fig. 2a). The red emission, on the other hand, is commonly attributed to excess oxygen on the ZnO surface[12, 15-17] The yellow emission for undoped ZnO nanorods prepared through hydrothermal growth can be due to the $Zn(OH)_2$ or OH group.[16] The increase in the relative intensity of yellow emissions as the doping concentration of Li was increased to 5 and 10 atom% can be due to both Li_{Zn} and Li_i in the ZnO crystal. The transitions from donor levels in the crystal (can be both from V_o or Li_i) to Li_{Zn} acceptor levels releases yellow emissions.[7, 14]

At 5 atom % doping, the peaks of the native defects (Zn_i and V_O) of ZnO remain relatively unchanged. Thus, the change in yellow emission intensity confirms the replacement of Zn by the smaller Li atom in the crystal. This is supported by the decrease of lattice parameter and ZnO crystal size as observed by XRD analysis (Fig. 1b,c). On the other hand, at 10 atom % doping, the green emission of the crystal significantly decreased and the yellow emission continued to increase. This indicates the reduction of V_O and a proliferation of Li impurity in the crystal. Li ions cannot substitute for O (Li_O) in the crystal lattice due to the high formation energy.[5] The Li ions can diffuse into the spaces in between the lattice (Li interstitial, Li_i). The diffusion of Li_i leads to an increase in both crystal size and lattice parameter as seen in Fig. 1. Interestingly, the red emission band, which relates to excess oxygen at the surface, becomes stronger as the Li content is increased to 10 atom % doping and decreased significantly for the heavily doped samples (not shown here). We believe that Li incorporation into ZnO can induce oxygen-enrichment of ZnO surfaces. The increase in red emission has also been observed in the case of Li-doped bulk ZnO.[14] In other words, the decrease in red emission for heavy doping can be attributed to the degradation of crystallinity as shown by the XRD spectra.

The placement of Li in the ZnO crystal was investigated by evaluating the first ionization energy (IE, Fig. 3) from the photoemission yield spectra (Fig. S4, ESI†). An increase of the IE is observed for $0 < x < 0.15$ atom % Li-doped ZnO nanorods. This is due to the acceptor action of the Li_{Zn} in the ZnO crystals. IE decreased upon further Li-doping. This can mean that the additional Li after 15 atom% is Li_i, due to the donor action of Li_i. For all doping concentrations studied, the measured IE is still higher than that of pure ZnO samples owing to the effect of Li_{Zn}. Increasing the doping concentration further however may lead to IE lower than that of the pure ZnO samples due to the effect of Li_i.

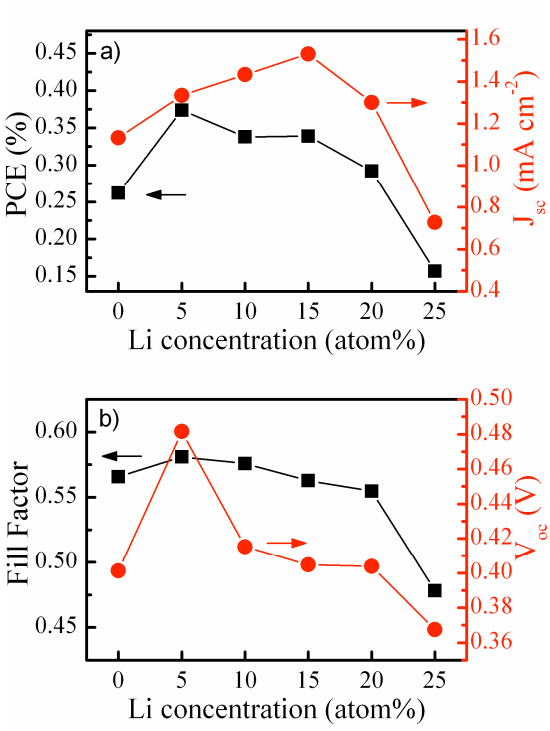

Fig. 5 The photovoltaic parameters, a) PCE, J_{sc}, and b) fill factor, V_{oc} of hybrid $Zn_{1-x}Li_xO$ nanorods/P3HT solar cells (x = 0 – 0.25).

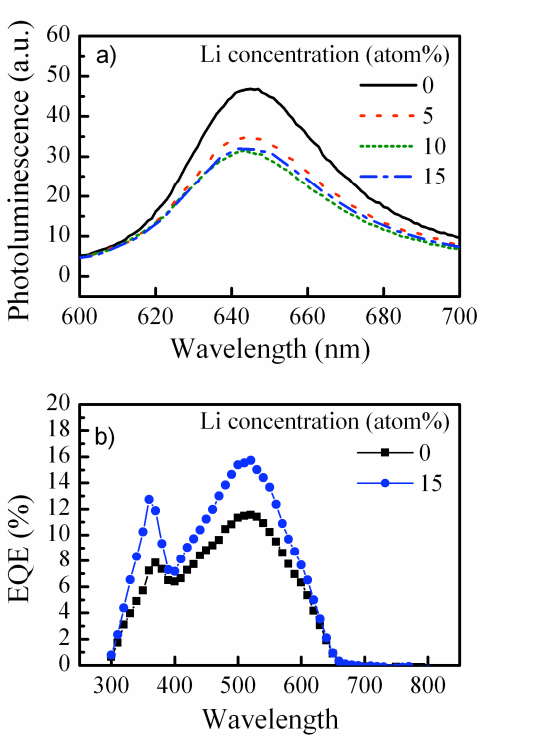

Fig. 6 a) photoluminescence of hybrid $Zn_{1-x}Li_xO$ nanorods/P3HT films on glass substrates (x = 0 – 0.15) and b) the EQE of hybrid $Zn_{1-x}Li_xO$ nanorods/P3HT solar cells (x = 0, 0.15)

The optical band gap of the films was determined from the absorption coefficient (Fig. S5, ESI†) of Li-doped ZnO nanorods. It was determined that the optical band gap of Li-doped ZnO nanorods is a direct optical transition. The values of the optical band gaps showed no change at around 3.30 eV as doping concentration was increased, as shown in Fig. 4. The effect to the photovoltaic characteristics will be discussed below.

Characteristic of hybrid Li-doped ZnO/P3HT solar cells

To observe the effect of Li incorporation into ZnO nanorods on the electrical properties and band edge of hybrid solar cells, $Zn_{1-x}Li_xO$ nanorods/P3HT devices were fabricated. Fig. 5 shows the performance of the devices as a function of Li concentration under AM1.5, 100 mW cm^{-2}. The Li incorporation to ZnO nanorods resulted to a systematic increase in short-circuit current density (J_{sc}) from 1.13 mA cm^{-2} for x = 0 to as high as 1.53 mA cm^{-2} for x = 0.15, as shown in Fig. 5a. With the further increase of Li concentration, the J_{sc} dropped significantly. Interestingly, the open-circuit voltage (V_{oc}) of the device with x = 0.05 have a significant value of 0.48 eV compared to that of the other devices. The fill factor (FF) shows no significant changes at low Li concentration. It starts to fall off after 15 atom%. Correspondingly, the power conversion efficiency (*PCE*) improves with increasing Li concentration, then falls off after x = 0.05, as seen in Fig. 5a. The highest PCE of 0.37% (J_{sc} 1.41 mA cm^{-2}, V_{oc} 0.48 eV, FF 0.55) was obtained at 5 atom % doping.

To investigate the origin of the enhancement on J_{sc}, the photoluminescence (PL) of $Zn_{1-x}Li_xO$/P3HT thin films and the external quantum efficiency (EQE) of the Li-doped devices were collected. In Fig. 6a, the quenching in PL intensity indicates efficient charge transfer at the $Zn_{1-x}Li_xO$ nanorods/P3HT interface when x = 0.10-0.15. This is attributed to the oxygen-enriched surface, as observed by the change of red emission in Fig. 2. The increase in oxygen concentration at the surface of inorganic semiconductors improves the performance of hybrid inorganic/organic solar cells.[18] This oxygen-enrichment of the surface is also observed when ZnO nanocrystallite aggregates are doped by Li atoms and show an improvement of photovoltaic performance for dye-sensitized solar cells.[19]

The external quantum efficiency (EQE) of the ITO/$Zn_{1-x}Li_xO$ nanorod/P3HT/Ag (x = 0, 0.15) devices are shown in Fig. 6b. The 15 atom % Li-doped ZnO nanorods device shows a maximum EQE of 16.0% at 520 nm, correspondong to J_{sc} of 1.53 mA cm^{-2}. A peak in the EQE spectra at around 520 nm is attributed to absorptions of P3HT and charge separation at ZnO/P3HT interfaces as observed by the quenching in PL intensity. A peak in EQE spectra at 370 nm is caused by the UV light absorption of ZnO and subsequent transfer of holes to P3HT.[20] The samples doped upto 15 atom % show an enhancement in these two peaks. The quenching in PL intensity and the enhancement of EQE confirm the effective charge transport at the interface.

The singularity of the improvement in V_{oc} obtained at 5 atom% was investigated. One possible cause of V_{oc} improvement is an upward shift of the conduction band to the vacuum level resulting from the broadening of the energy gap after Li doping. The broadening of the energy band gap was previously observed for the case of a planar bilayer ZnMgO/P3HT system.[3] The V_{oc} increased because of the larger difference between the conduction band of the acceptor and highest occupied molecular orbital (HOMO) of the donor. However, in our system, a constant optical band gap for Li-doped ZnO nanorod thin films (Fig. 4) was observed, thus this could not be the case of the increased V_{oc} for 5 atom% Li-doped nanorods.

Another cause of V_{oc} improvement is the upward shift of the conduction band to vacuum level caused by the lowering of Fermi energy level.[21] The trend of changes in Fermi level follow the IE trend with Li doping. From Fig. 3, the trend predicted V_{oc} to increase from x = 0 to x = 0.15 and decrease for heavy doping. However, the actual V_{oc} obtained in Fig. 5b did not follow this prediction accurately. Factors that can cause disparity from the predicted values are probably injected dark current, minority carriers in the materials, charge recombination, etc.[3]

To investigate this further, the current density-voltage (*J-V*) curves for the hybrid devices were fitted using a single diode model with the equation:[22]

$$J = J_0\left\{\exp\left(\frac{V - JR_SA}{nkT/e}\right) - 1\right\} + \frac{V - JR_SA}{R_PA} - J_{ph} \qquad (1)$$

where J is the current density, J_0 is the diode reverse saturation current density, J_{ph} is the light-generated current density, q is the electronic charge, V is the applied voltage, A is the device active area, R_S is the series resistance, n is the ideality factor, k is Boltzmann's constant, T is temperature, and R_P is the shunt resistance. The single diode model fitting is an effective method to investigate the effect of specific aspects in solar cells since the parameters of the model can be related to different mechanisms in power conversion. The *J-V* characteristics for all devices were found to fit the model well (Fig. S6, ESI†). The parameters extracted from the fits are shown in Fig. 7.

The diode reverse saturation current density (J_0) is lower for 5 atom % Li-doped device by a factor of 2.7, compared to pure ZnO devices. Then, it increased with increasing Li conconcentration. The origin of J_0 can be from the charge injection at the surface of the electrodes and the presence of minority carriers in the materials.

At the ITO/$Zn_{1-x}Li_xO$ interfaces, charge injection from the ITO electrode to the ZnO nanorods can occur under forward bias. This injected current can be suppressed if the barrier at ITO/ZnO is stronger. The strength of this barrier is increased by the shift of the conduction band upward to the vacuum level. This behavior is also observed incase of ITO/$Zn_{1-x}Li_xO$/Au diodes.[21] From the Fermi level trend, charge injection is expected to decrease for the case of x = 0.10-0.15 devices, since their work functions are smaller than that of the x = 0.05 device, but this did not happen. This irregularity can be explained by the effect of minority carriers (holes) in ZnO crystals. The presence of Li_{Zn} results to higher hole density. Since the Li element is inhomogeniously distributed in ZnO, the majority and minority carriers are also inhomogeniously distributed. Hole carriers can diffuse and drift from the Li-rich region (top of nanorod) to the electrode (negatively charged) under forward bias, increasing reverse current density. We believe that the suppression of charge injection dominates the effect of minority charge in the case of 5 atom % doping, causing its J_0 to become smaller. The increase of J_0 at x > 0.10 doping reduces the predicted V_{oc} values.

The increase of ideality factor with the increase of Li concentration was observed, as seen in Fig. 7. This indicates an increase the charge recombination in the devices. The increase in n value can be due to the occurrence of trap-assisted recombination mechanism,[23] wherein a photogenerated electron

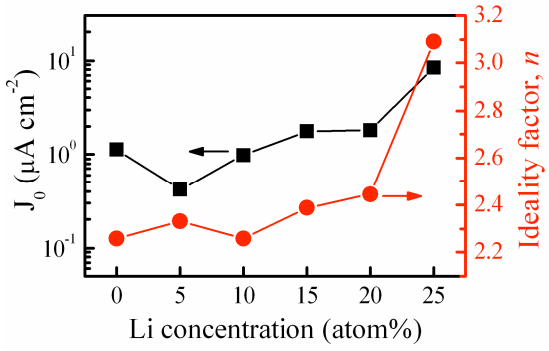

Fig. 7 Reverse current density (J_0) and ideality factor (n) of hybrid $Zn_{1-x}Li_xO$ nanorods/P3HT solar cells (x = 0 – 0.25).

in conduction band falls into a trap, which is caused by the present of Li impurity, and recombine with holes generated by the defect. This recombination downgrades the device performance, especially the value of fill factor.

Conclusions

We have shown a method for the enhancement in photovoltaic performance of hybrid solar cells constructed from ZnO nanorods and P3HT by Li incorporation to ZnO crystal. The difference in photovoltaic properties brought about by Li doping were determined from concentrations of the precursor solution by normalized photoluminescence and first iornization energy analyses. The presence of Li_{Zn} in ZnO crystals has been observed at 5 atom% and the satutration of Li_{Zn} was observed at 15 atom%. The Li_i concentration started increasing at 10 atom% and additional Li atom would tend to be Li_i rather than Li_{Zn} after 15 atom%. The oxygen-enrichment of ZnO surface caused by Li doping, observed by red PL emission, yields the effective charge transfer at the interface. This leads to the enhancement of J_{sc}. The obtained improvement of V_{oc} was obtained. This is attributed to the suppression of the charge injection from the electrode brought about by the increase in barrier height at the ITO/ZnO interface. However, further Li_{Zn} leads to increased reverse current densities of minority carriers decreasing V_{oc} after the maximum value at 5 atom% incorporation. The maximum power conversion efficiency of 0.37% was obtained at 5 atom% doping.

Acknowledgements

The authors are grateful to Dr.Taro Sonobe for the use of photolominescence measurements. The work was supported by the New Energy and Industrial Technology Development Organization (NEDO) of the Ministry of Economy, Trade, and Industry (METI), and Core Research of Evolutional Science & Technology Agency (CREST) from Japan Science Technology Agency (JST).

Notes and references

Institute of Advanced Energy, Kyoto University, Uji, Kyoto, 611-0011, Japan. Fax: +81-774-38-3508; Tel: +81-774-38-4520;
E-mail: t-sagawa@iae.kyoto-u.ac.jp, s-yoshi@iae.kyoto-u.ac.jp

† Electronic Supplementary Information (ESI) available: Experimental detail of the characterization and analysis (SREM-Eels, XRD, optical energy gap, PYS, and *JV* fitting). See DOI: 10.1039/b000000x/

1. P. Ravirajan, A. M. Peiro, M. K. Nazeeruddin, M. Graetzel, D. D. C. Bradley, J. R. Durrant and J. Nelson, *J. Phys. Chem. B*, 2006, **110**, 7635-7639.
2. T. Rattanavoravipa, T. Sagawa and S. Yoshikawa, *Sol. Energ. Mat. Sol. C*, 2008, **92**, 1445-1449.
3. D. C. Olson, S. E. Shaheen, M. S. White, W. J. Mitchell, M. F. A. M. van Hest, R. T. Collins and D. S. Ginley, *Adv. Funct. Mater.*, 2007, **17**, 264-269.
4. I. Gonzalez-Valls and M. Lira-Cantu, *Energ. Environ. Sci.*, 2009, **2**, 19-34.
5. M. G. Wardle, J. P. Goss and P. R. Briddon, *Phys. Rev. B*, 2005, **71**, 155205.
6. M. Joseph, H. Tabata and T. Kawai, *Appl. Phys. Lett.*, 1999, **74**, 2534-2536.
7. M. D. McCluskey and S. J. Jokela, *J. Appl. Phys.*, 2009, **106**, 071101.
8. G. Srinivasan, R. T. R. Kumar and J. Kumar, *J Sol-Gel Sci Techn*, 2007, **43**, 171-177.
9. S. Fujihara, C. Sasaki and T. Kimura, *J. Eur. Ceram. Soc.*, 2001, **21**, 2109-2112.
10. M. K. Patra, K. Manzoor, M. Manoth, S. R. Vadera and N. Kumar, *J Lumin.*, 2008, **128**, 267-272.
11. D. H. Zhang, Z. Y. Xue and Q. P. Wang, *J. Phys. D Appl. Phys.*, 2002, **35**, 2837-2840.
12. B. Panigrahy, M. Aslam, D. S. Misra, M. Ghosh and D. Bahadur, *Adv. Funct. Mater.*, 2010, **20**, 1161-1165.
13. K. Vanheusden, C. H. Seager, W. L. Warren, D. R. Tallant and J. A. Voigt, *Appl. Phys. Lett.*, 1996, **68**, 403-405.
14. N. Ohashi, T. Nakata, T. Sekiguchi, H. Hosono, M. Mizuguchi, T. Tsurumi, J. Tanaka and H. Haneda, *Jpn. J. Appl. Phys. 2*, 1999, **38**, L113-L115.
15. X. L. Wu, G. G. Siu, C. L. Fu and H. C. Ong, *Appl. Phys. Lett.*, 2001, **78**, 2285-2287.
16. A. B. Djurisic, Y. H. Leung, K. H. Tam, Y. F. Hsu, L. Ding, W. K. Ge, Y. C. Zhong, K. S. Wong, W. K. Chan, H. L. Tam, K. W. Cheah, W. M. Kwok and D. L. Phillips, *Nanotechnology*, 2007, **18**, 095702.
17. T. Chen, G. Z. Xing, Z. Zhang, H. Y. Chen and T. Wu, *Nanotechnology*, 2008, **19**, 435711.
18. D. C. Olson, S. E. Shaheen, R. T. Collins and D. S. Ginley, *J. Phys. Chem. C*, 2007, **111**, 16670-16678.
19. Q. F. Zhang, C. S. Dandeneau, S. Candelaria, D. W. Liu, B. B. Garcia, X. Y. Zhou, Y. H. Jeong and G. Z. Cao, *Chem. Mater.*, 2010, **22**, 2427-2433.
20. D. C. Olson, J. Piris, R. T. Collins, S. E. Shaheen and D. S. Ginley, *Thin Solid Films*, 2006, **496**, 26-29.
21. M. T. Lloyd, Y. J. Lee, R. J. Davis, E. Fang, R. M. Fleming, J. W. P. Hsu, R. J. Kline and M. F. Toney, *J. Phys. Chem. C*, 2009, **113**, 17608-17612.
22. S. Choi, W. J. Potscavage and B. Kippelen, *J. Appl. Phys.*, 2009, **106**, 054507.
23. O. Tuzun, S. Oktik, S. Altindal and T. S. Mammadov, *Thin Solid Films*, 2006, **511**, 258-264.

Supporting Information

Vertically-Aligned ZnO Nanorods Doped with Lithium for Polymer Solar Cells: Defect Related Photovoltaic Properties

Pipat Ruankham, Takashi Sagawa,* Horoshi Sakaguchi and Susumu Yoshikawa*

Institute of Advanced Energy, Kyoto University, Uji, Kyoto, 611-0011, Japan

Corresponding Authors: t-sagawa@iae.kyoto-u.ac.jp, s-yoshi@iae.kyoto-u.ac.jp

A. Energy-Loss Spectroscopy in a Scanning Transmission Electron Microscope (STEM-EELS) Study

In order to investigate the presence of Li atom in ZnO nanorod arrays, the 25 atom% Li doped ZnO nanorods was chosen as sample for STEM-EELs study. The Li element maps, in Figure S1, show that Li-rich phase is on the top of ZnO nanorods, confirming the Li incorporation into ZnO crystal during hydrothermal growth.

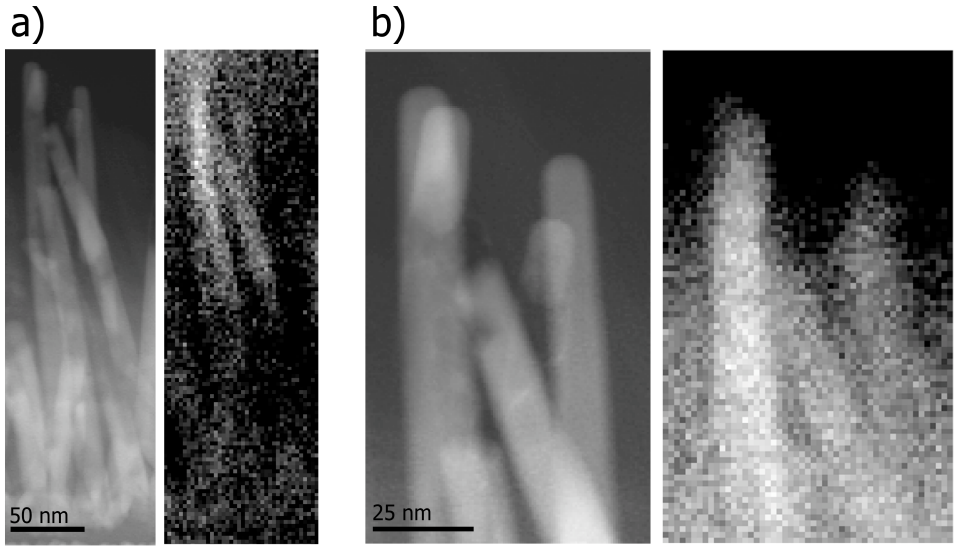

Fig. S1 The STEM image (left) and Li map (right) of 25 atom% Li doped ZnO nanorods, with scale bar a) 50 nm and b) 25 nm.

B. X-ray Diffraction (XRD) Analysis

The XRD patterns of ZnO nanorods with different Li-doping concentration on ITO substrates are shown in Figure S2.

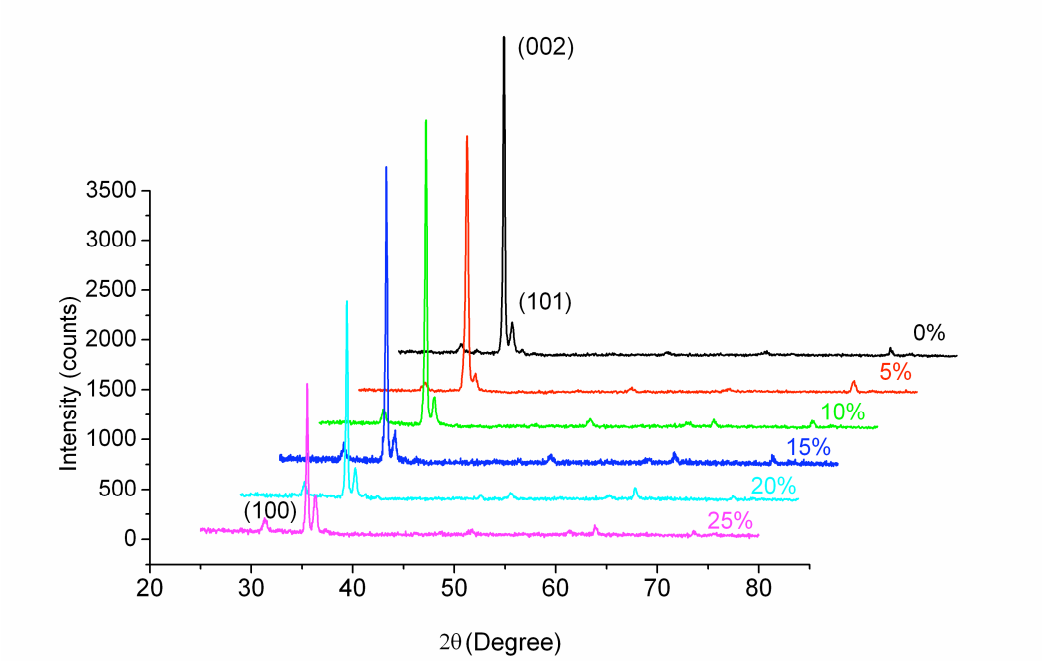

Fig. S2 The XRD patterns of $Zn_{1-x}Li_xO$ nanorods.

To better approximate the position and the FWHM of XRD peaks, XRD spectra were characterized using the Peak Fitting module. The crystal size (D) was calculated from the (002) peak width by using the Scherrer's equation

$$D = \frac{0.9\lambda}{\beta_{1/2}\cos(\theta)} \quad (1)$$

where D, λ, $\beta_{1/2}$ and θ are the mean crystal size, the X-ray wavelength, full-width at haft-maximum (FWHM) and Bragg diffraction angle, respectively. The lattice parameter of *c* was calculated using Equation (2) for the film:

$$\frac{1}{d^2} = \frac{4}{3}\left(\frac{h^2 + hk + k^2}{a^2}\right) + \frac{l^2}{c^2} \quad (2)$$

where *d* is lattice spacing, *a* and *c* are lattice parameters.

C. Room Temperature Photoluminescence of $Zn_{1-x}Li_xO$ Nanorods

Photoluminescence studies were carried out using a He-Cd laser operating at wavelength of 325 nm. The PL spectra of Li-doped ZnO nanorods at various Li content are shown in Figure S3. These spectra can be divided by Gaussian fitting.

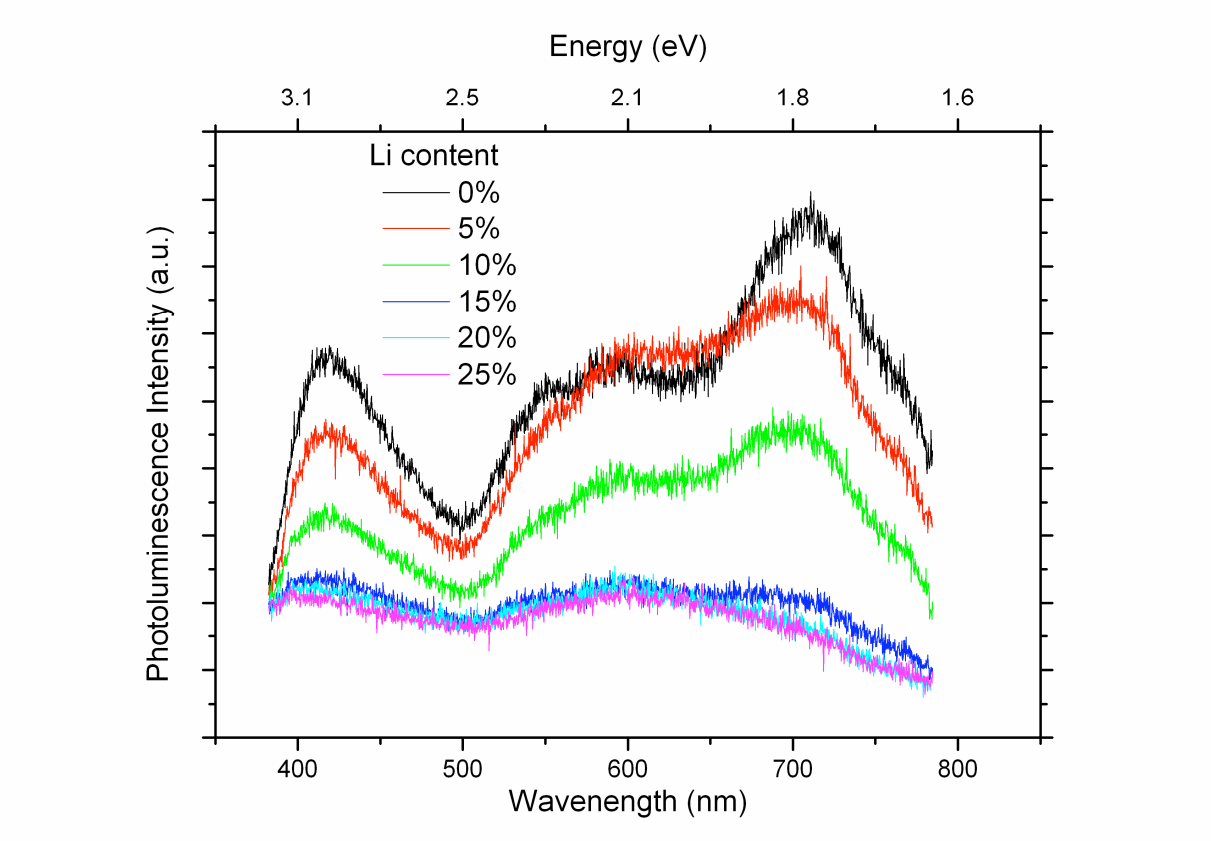

Fig. S3 The PL spectra of Li-doped ZnO nanorods at various Li content (0% - 25%)

D. Photoemission Yield Spectroscopy in Air (PYS) Study

In order to understand the electric conductivity due to the Li incorporation, the PYS were performed in air with the Riken Keiki AC-2 system, which are shown in Figure S5. Threshold energy of photoemission corresponds to the first ionization potential.

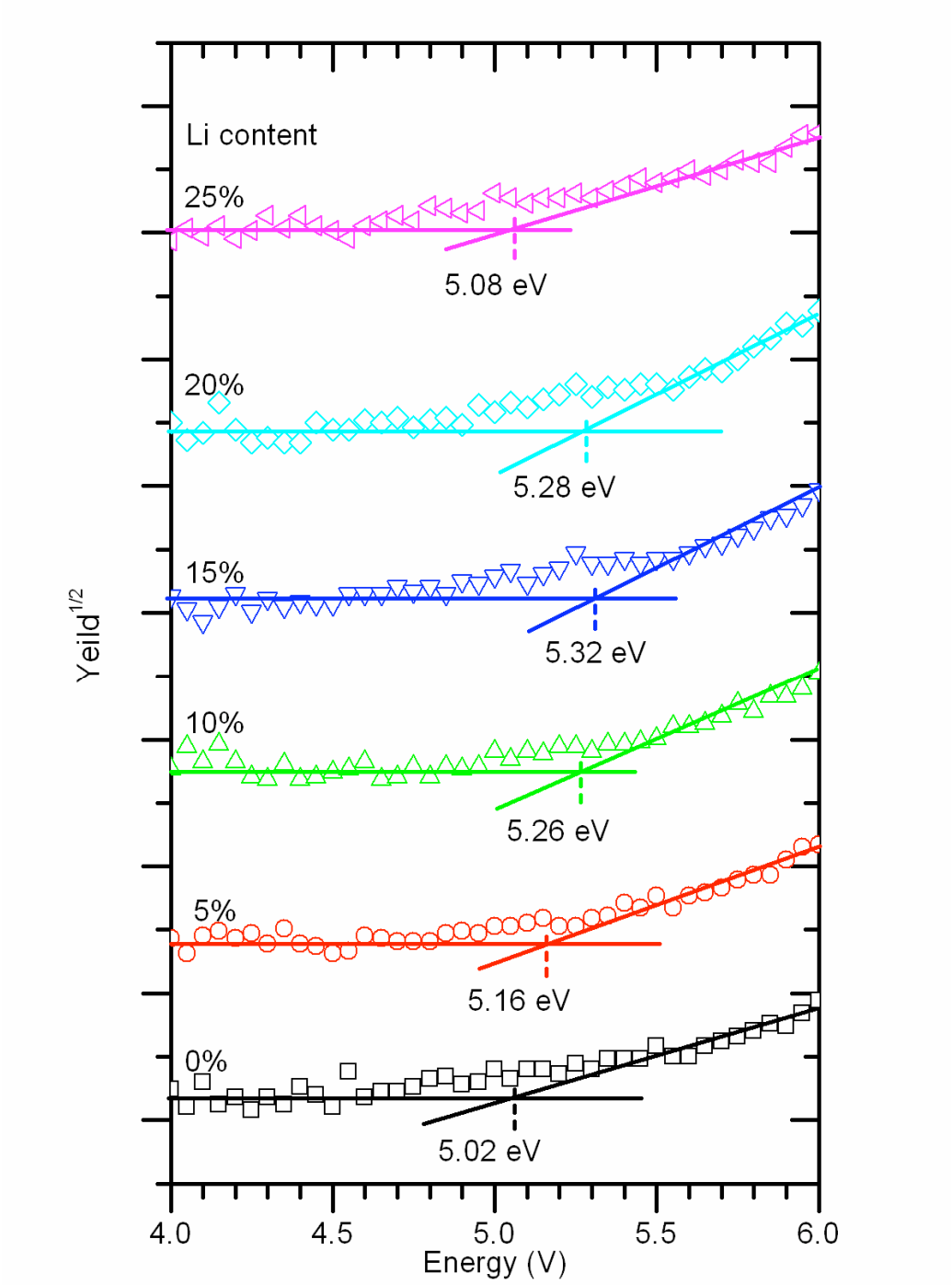

Fig. S4 Photoemission yield of Li-doped ZnO nanorods at various concentration of dopant

E. Optical Energy Gap Measurement

Transmittances and absorbances of Li doped ZnO nanorods coated on glass substrate were collected using UV-vis spectrophotometer (UV-2450 SHIMADZU), as shown in Figure S4.

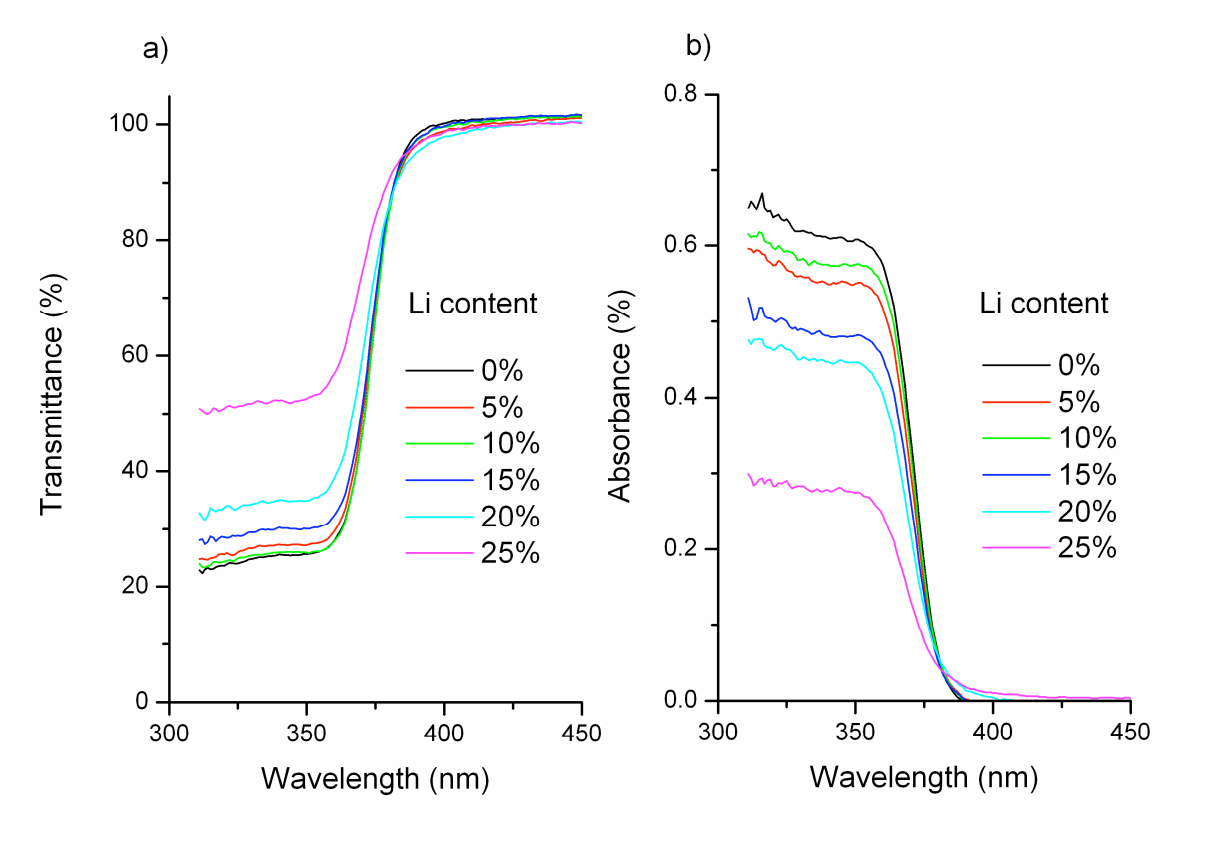

Fig. S5 Transmittances and absorbances of Li doped ZnO nanorods at various Li content coated on glass substrate.

The absorption coefficient (α) was calculated from Lambert-Beer-Bouguer law ;

$$\alpha = \frac{1}{d}\ln\left(\frac{1}{T}\right) \quad (3)$$

where d and T is thickness of the film and transmittance, respectively. The optical band gap of the films was determined using Equation (4) (S. M. Sze, Physics of Semiconductor Devices ,Wiley-Interscience, 2006);

$$\alpha = A(h\nu - E_g)^m \quad (4)$$

where ν, E_g and m are wavelength, optical energy gap and constant which determines types of optical transition (m = 1/2 for allowed direct transition and m = 2 for allowed indirect transition).

F. Fitting of Current-Voltage Characteristics by Equivalent Circuit Model

To investigate the effect of Li incorporation into ZnO crystal on photovoltaic performance, the single diode model (S. Choi, W. J. Potscavage, B. Kippelen, J. Aapl. Phys. 2009, 106) was performed by Equation (5);

$$J = J_0\left\{\exp\left(\frac{V - JR_S A}{nkT/e}\right) - 1\right\} + \frac{V - JR_S A}{R_P A} - J_{ph} \quad (5)$$

where J is the current density, J_0 is the diode reverse saturation current density, J_{ph} is the light-generated current density, q is the electronic charge, V is the applied voltage, A is the device active area, R_S is the series resistance, n is the ideality factor, k is Boltzmann's constant, T is temperature, and R_P is the shunt resistance. The fitting parameters were J_0, n, R_S, R_P. The J-V characteristics for all devices were fitted well as shown in Figure S6.

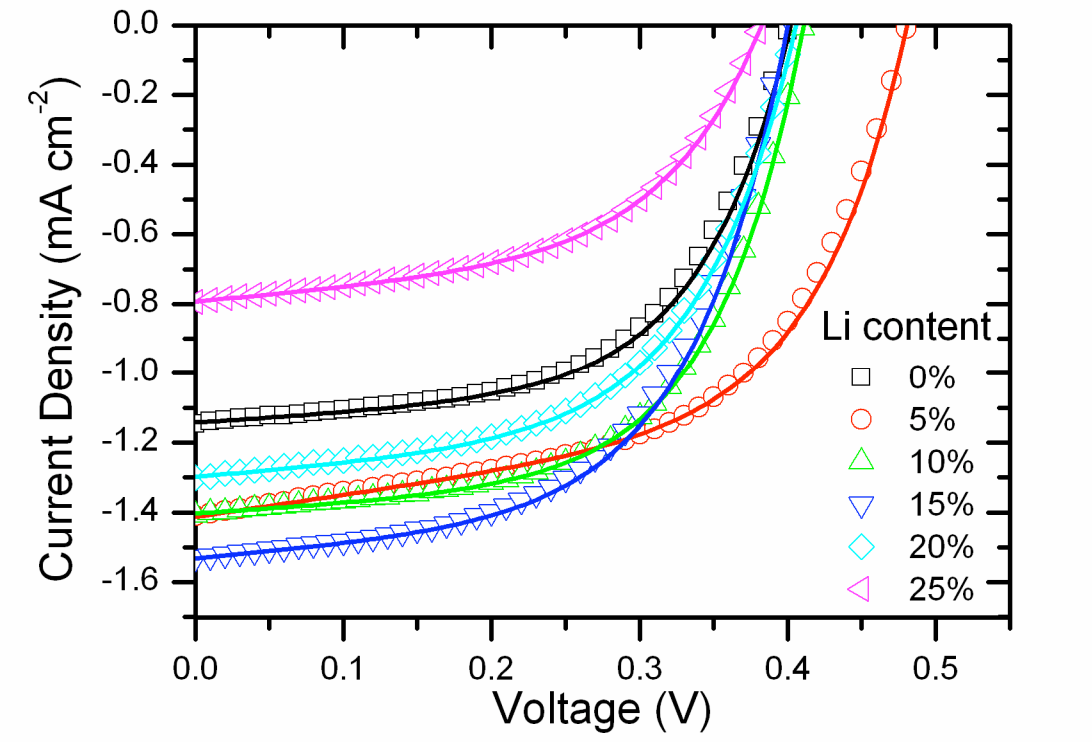

Fig. S6 Experimental (shapes) and fitted (solid lines) J-V characteristics for hybrid Li-doped ZnO nanorod/P3HT solar cell under illumination.

Reference

1 B.D. Cullity; S.R. Stock, *Element of X-ray Diffraction*, 3rd ed., Prentice Hall, 2001

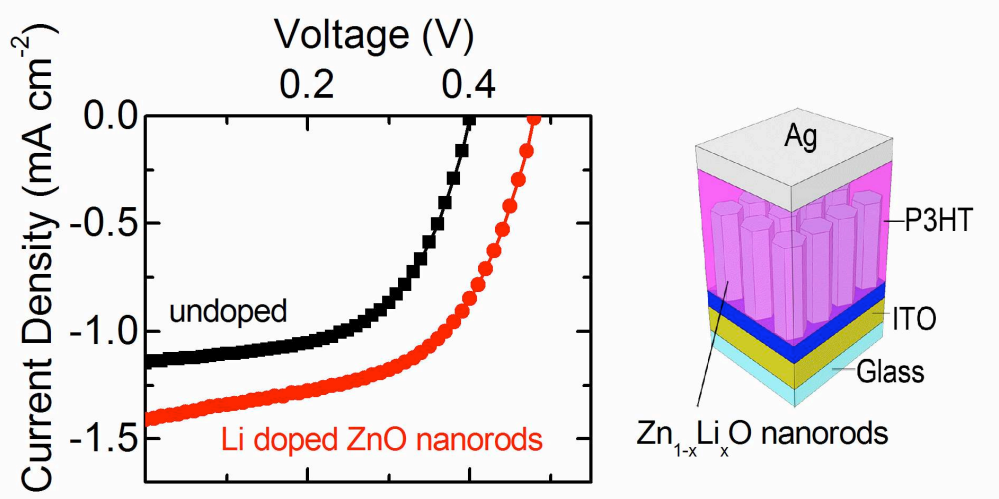

79x39mm (600 x 600 DPI)

Li-doped ZnO nanorods for hybrid photovoltaic application (ITO/Li-ZnO/P3HT/Ag) as electron acceptors improved power conversion efficiency from 0.26%(undoped) to 0.37%.

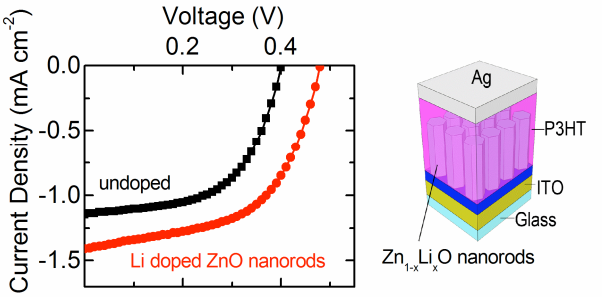

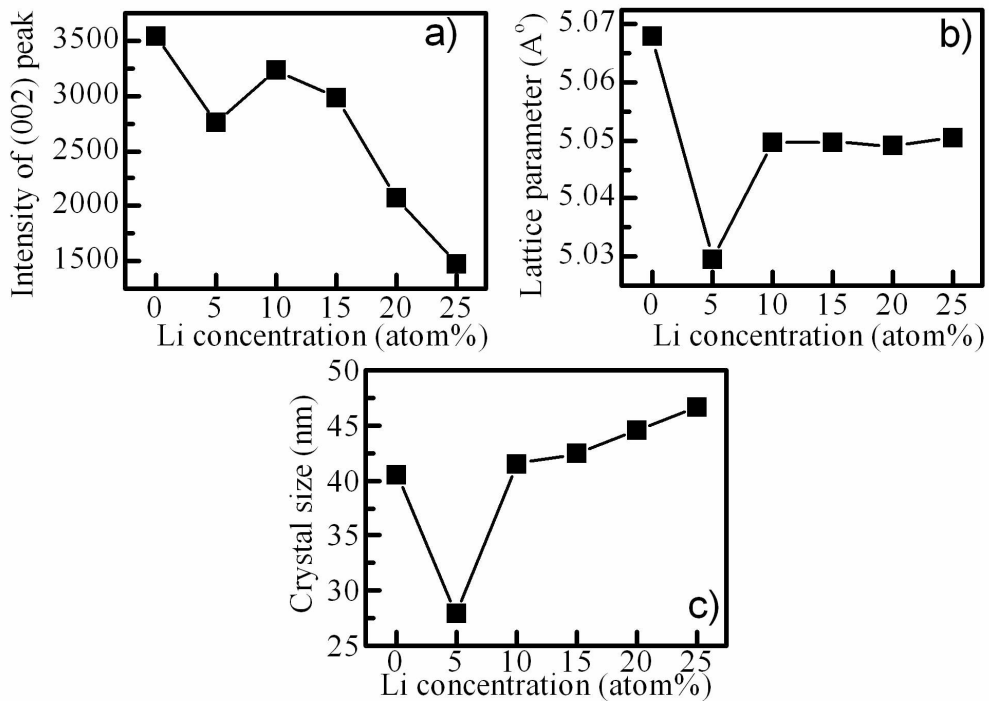

The variation of a) (002) peak intensity, b) lattice parameter c, and c) crystal size of ZnO nanorods doped by various Li concentration.
82x58mm (600 x 600 DPI)

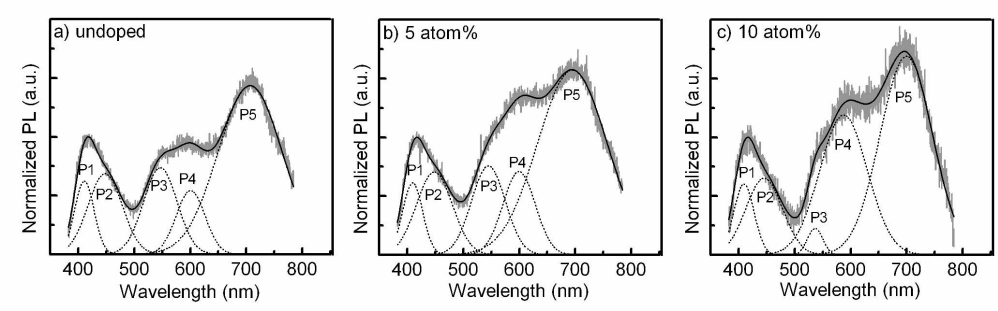

The normalized of room temperature photoluminescence for Zn1-xLixO nanorod films on glass substrates for a) undoped, b) x = 0.05, and c) x = 0.10. The gray solid lines present the experimental data. The P1-P5 (dot lines) denotes the ultraviolet emission, blue emission, green emission, yellow emission, and red emission, respectively. The black solid line is the summation of P1-P5.
175x55mm (600 x 600 DPI)

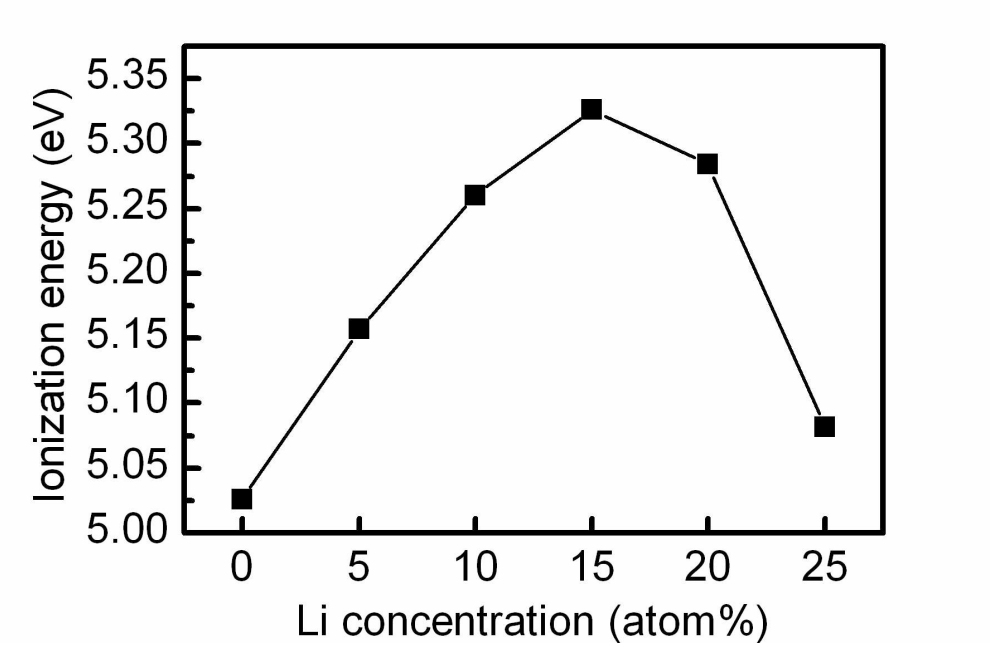

The first ionization energy (IE) of Zn1-xLixO nanorod films.
75x49mm (600 x 600 DPI)

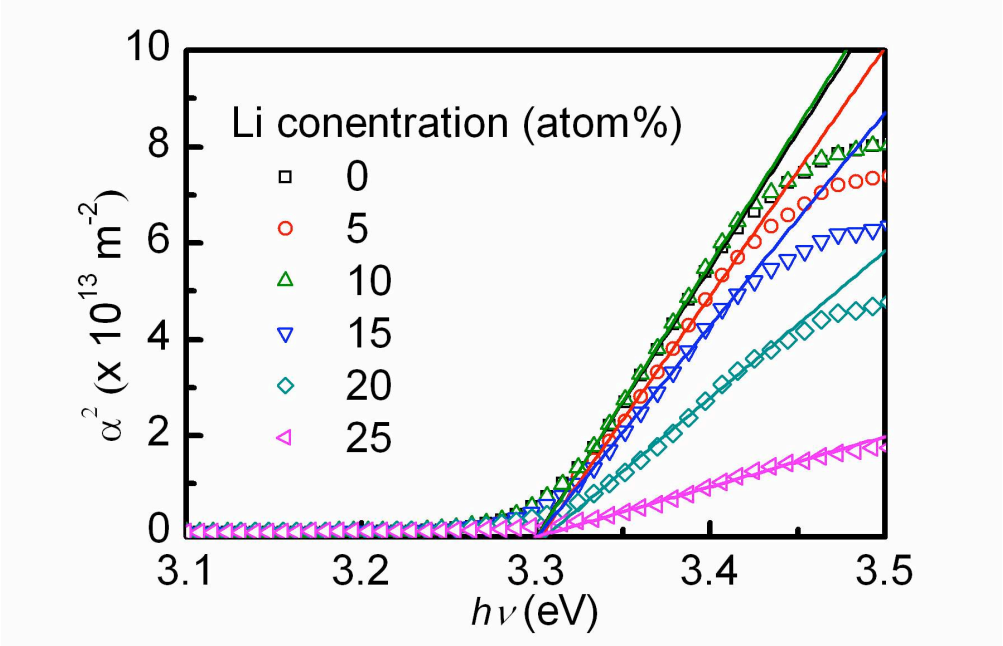

The plot of absorption coefficient (α) versus photon energy (hν) for Zn1-xLixO nanorod films (x = 0-0.25) on glass substrates. The open symbol and solid line denote the experimental data and fitted curve from equation (ESI†)
75x49mm (600 x 600 DPI)

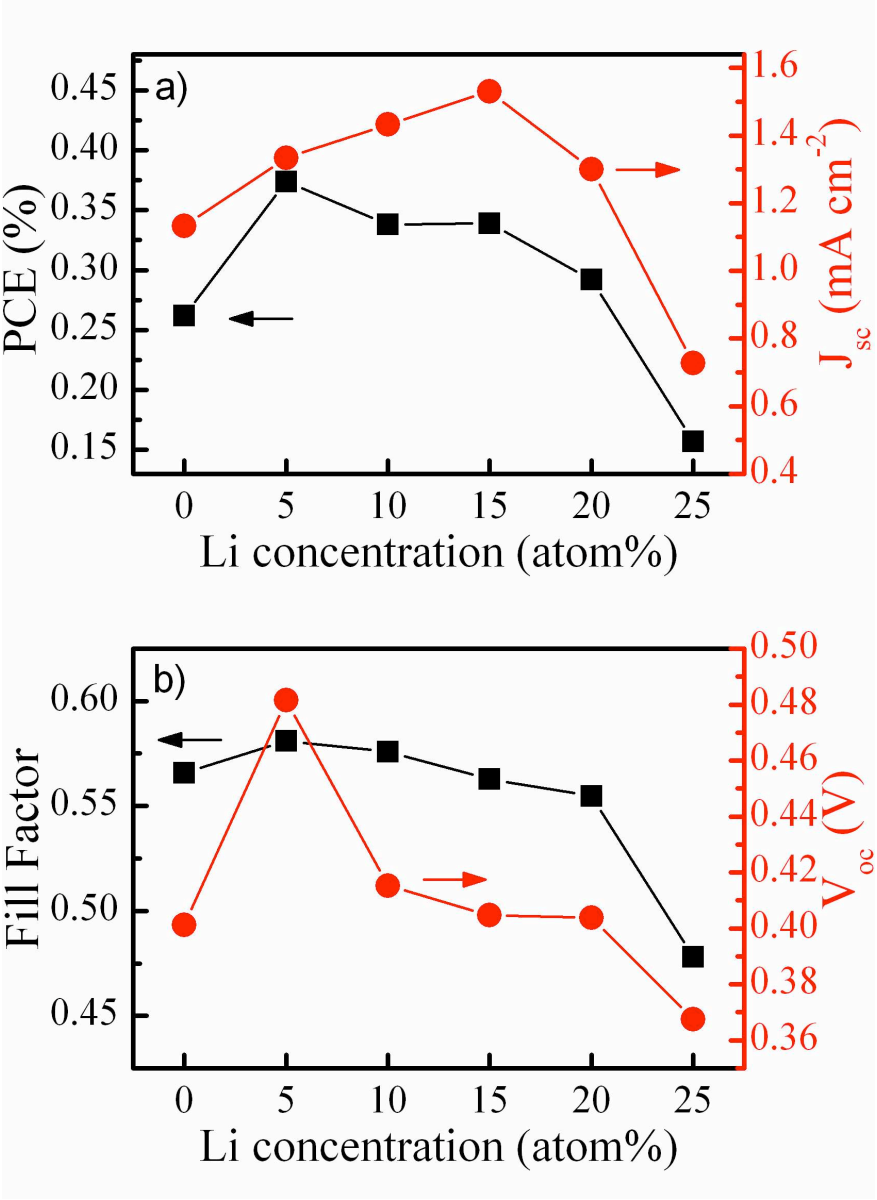

The photovoltaic parameters, a) PCE, Jsc, and b) fill factor, Voc of hybrid Zn1-xLixO nanorods/P3HT solar cells (x = 0 – 0.25).
71x98mm (600 x 600 DPI)

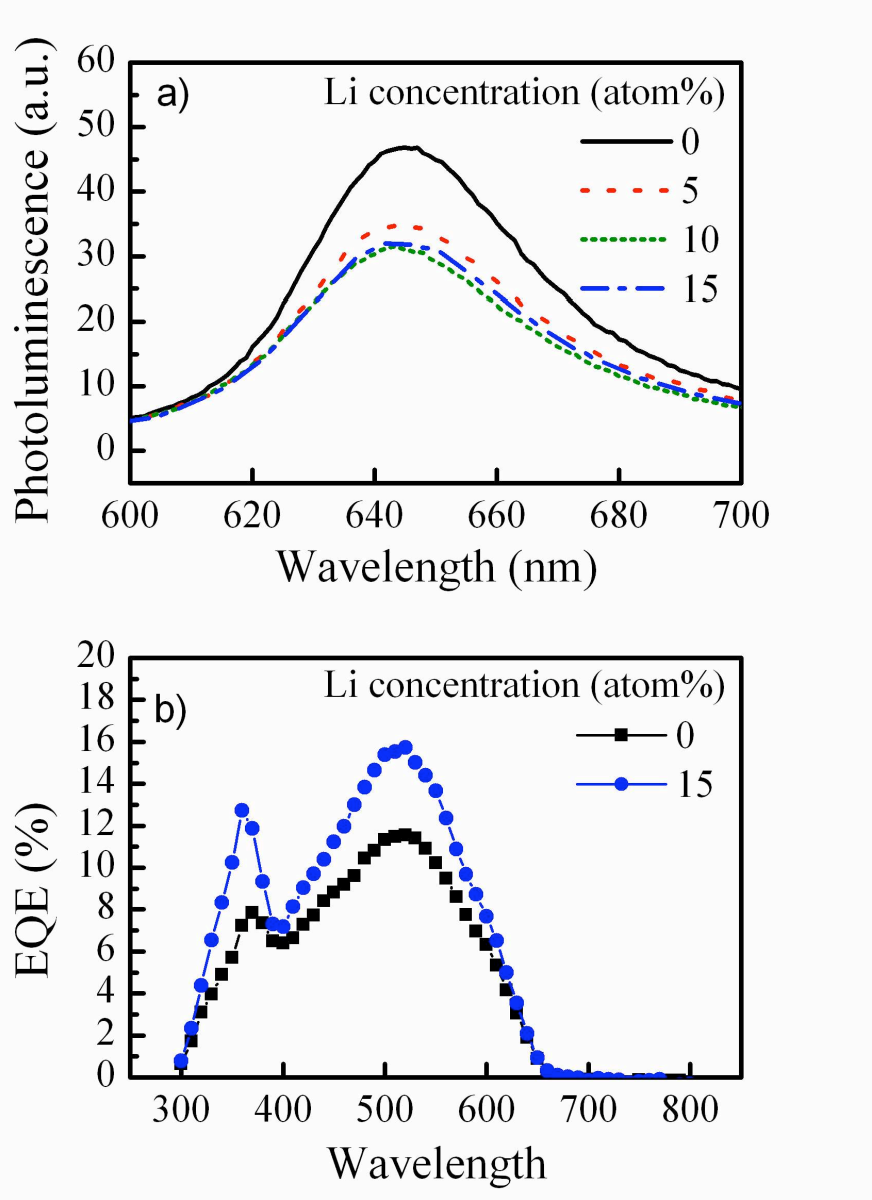

a) photoluminescence of hybrid Zn1-xLixO nanorods/P3HT films on glass substrates (x = 0 – 0.15) and b) the EQE of hybrid Zn1-xLixO nanorods/P3HT solar cells (x = 0, 0.15)
71x98mm (600 x 600 DPI)

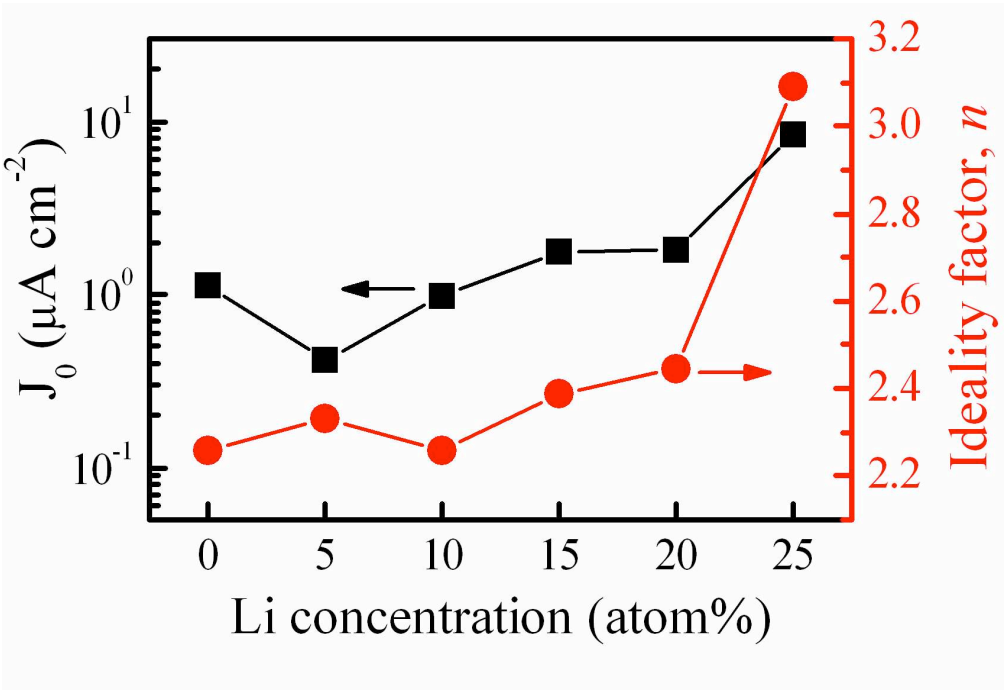

Reverse current density (J0) and ideality factor (n) of hybrid Zn1-xLixO nanorods/P3HT solar cells (x = 0 – 0.25).
71x49mm (600 x 600 DPI)